Article

Single-antenna super-resolution positioning with nonseparable toroidal pulses

Check for updates

Ren Wang [1,2] ✉, Pan-Yi Bao[1], Xiaoyu Feng[1], Junpu Wu[1], Bing-Zhong Wang[1] & Yijie Shen [3,4] ✉

The fundamental principle of satellite/node-based positioning involves triangulating the receiver's coordinates through the intersection of spatial distances. Advancements in hybrid wireless networks have yielded high-precision positioning at decimeter-level (wavelength-level), approaching the resolution limits in free space. Here we present a 3D super-resolution positioning paradigm in free space by utilizing a kind of topologically structured pulses, toroidal electromagnetic pulses. We demonstrate that the space-time nonseparability and skyrmion topology inherent in toroidal pulses can be harnessed to achieve freespace microwave 3D positioning with super-resolution accuracy, reaching the centimeter level, using a single emitting antenna. This work opens up avenues for exploring the potential applications of topological electromagnetic pulses including but not limited to positioning, imaging and sensing technologies.

Freespace wireless microwave positioning plays a crucial role in daily life and scientific research[1–4]. Satellite navigation systems, such as the Global Positioning System (GPS), have revolutionized global navigation, mobile communication, and automated driving[5–7]. Recent advancements have led to the development of node network-based positioning systems by replacing satellite transmitters with ground-based stations or network nodes, thereby enhancing the precision and adaptability of positioning systems[8–11]. Both node network-based and satellite-based positioning systems rely on the multi-transmitter positioning paradigm and spatial distance intersection principle, illustrated in Fig. 1a. However, two challenges, accuracy and node number, pose significant hurdles in freespace microwave positioning scenarios. Firstly, the precision of positioning based on the spatial distance intersection principle depends on synchronization and ranging. Typically, the synchronization accuracy of GPS systems reaches several nanoseconds, resulting in meter-level positioning errors. Recent advancements in hybrid wireless networks have pushed synchronization precision to sub-nanosecond levels, enabling decimeter-level (wavelength-level) high-accuracy positioning[10,11]. This development approaches the resolution limits in free space and the accuracy is difficult to further enhance. Secondly, when accurately measuring flying time or distance l, each transmitter can only ascertain that the receiver lies on a sphere with a radius of l. Consequently, it is impossible to determine the 3D coordinates of a target using a single transmitting antenna based on the spatial distance intersection principle.

Topological electromagnetic fields exhibit vast potential applications in information and energy transmission[12–18] and super-resolution metrology or microscopy[19–24], thereby offering a potential avenue for achieving precise 3D positioning based on a single transmission antenna in free space. In 1996, Hellwarth and Nouchi introduced toroidal pulses, an exact solution to Maxwell's equations[25], which possess complex non-transverse skyrmion topological structures[26–29], space-time nonseparability[30–33], and strong interactions with matter[34,35]. Recently, electromagnetic toroidal pulses have been successfully generated in the optics, terahertz, and microwave[36–38], laying the foundation for their practical applications. However, to the best of our knowledge, there have been no reports of successful experimental implementations of toroidal pulses until now.

In this paper, we present a method for freespace microwave 3D positioning based on the space-time nonseparability and skyrmion topology of toroidal pulses, enabling 3D spatial positioning with super-resolution accuracy, reaching the centimeter level, using a single emitting antenna. The effectiveness of this method is validated through both theoretical analysis and experimental verification. As a result, the proposed methodology utilizing toroidal pulses lays the groundwork for a positioning paradigm.

Results

Positioning principle based on nonseparable toroidal pulses
The space-time nonseparability and space-polarization nonseparability of toroidal pulses, evident in their analytical expressions, are the fundamental

[1]Institute of Applied Physics, University of Electronic Science and Technology of China, Chengdu, 611731, China. [2]Yangtze Delta Region Institute (Huzhou), University of Electronic Science and Technology of China, Huzhou, 313098, China. [3]Centre for Disruptive Photonic Technologies, School of Physical and Mathematical Sciences, Nanyang Technological University, Singapore, 637371, Singapore. [4]School of Electrical and Electronic Engineering, Nanyang Technological University, Singapore, 639798, Singapore. ✉e-mail: rwang@uestc.edu.cn; yijie.shen@ntu.edu.sg

1
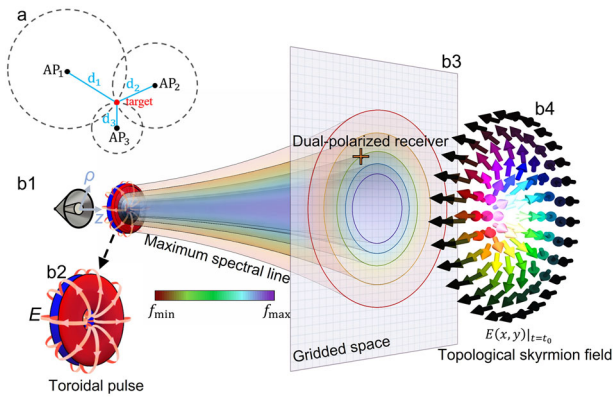
Fig. 1 | Schematic diagram of 3D positioning method based on toroidal pulses.
a Traditional spatial distance intersection principle, where AP represents access point; **b1** Toroidal pulses emission antenna; **b2** Electric field distribution of TM toroidal pulses, with the electric field E indicated by encircling pink arrows; **b3** Schematic diagram of the maximum frequency positioning and polarization distribution of toroidal pulses. We annotate the maximum positioning of the single-frequency field distribution in the ρ direction (referred to as the maximum spectrum line) using solid lines of different colors (from violet to red indicating from high to low frequencies). After spatial discretization, the maximum spectrum lines intersect with circular coils on a plane perpendicular to the propagation axis (z-axis). The correspondence between spatial and frequency spectra enables the determination of target coordinates (ρ, z). **b4** Skyrmion topology in toroidal pulses. The azimuthal coordinate θ of the target can be established based on the polarization characteristics of the electric field vector.

principles underlying the proposed 3D positioning method. The expression for the field distribution of transverse-magnetic (TM) toroidal pulses (Fig. 1b1, b2) in a cylindrical coordinate system is as follows[25]:

$$H_\theta = 4if_0 \frac{\rho(q_1 + q_2 - 2ict)}{[\rho^2 + (q_1 + i\tau)(q_2 - i\sigma)]^3} \quad (1)$$

$$E_\rho = 4if_0 \sqrt{\frac{\mu_0}{\varepsilon_0}} \frac{\rho(-q_1 + q_2 - 2iz)}{[\rho^2 + (q_1 + i\tau)(q_2 - i\sigma)]^3} \quad (2)$$

$$E_z = -4f_0 \sqrt{\frac{\mu_0}{\varepsilon_0}} \frac{\rho^2 - (q_1 + i\tau)(q_2 - i\sigma)}{[\rho^2 + (q_1 + i\tau)(q_2 - i\sigma)]^3} \quad (3)$$

where, H_θ is the magnetic field component in the θ direction, E_ρ and E_z are the electric field components in the ρ and z directions, respectively. The i denotes the imaginary unit, f_0 represents a real constant, q_1 and q_2 are adjustable real positive parameters, c represents the speed of light, t denotes time, $\tau = z - ct$, $\sigma = z + ct$. μ_0 and ε_0 represent the permeability and permittivity in vacuum, respectively.

Due to the inability to separate the spatial variable ρ from the temporal variable t in the expression of toroidal pulses mentioned above, their field equations cannot be expressed as spatial field forms with the temporal variable eliminated or temporal field forms with the spatial variable eliminated. This unique characteristic is referred to as space-time nonseparability, which is equivalent to space-frequency nonseparability. Due to their space-time nonseparability, toroidal pulses exhibit distinct electromagnetic fields in both the temporal and frequency domains at each spatial location[32]. When examining the maximum field distribution of toroidal pulses at a specific frequency point as it varies with the propagation space, we obtain a distribution of maximum spectral lines as shown in Fig. 1b3. The solid lines represent the radial maximum values of the E_ρ component along the z-axis for several frequencies ranging from f_{max} to f_{min}, with decreasing frequency from the inner to the outer regions. The maximum spectral lines are mutually separated and never intersect, which is one manifestation of the space-time nonseparability of toroidal pulses[32]. This spatial-frequency

correspondence forms the foundation for positioning based on the space-time nonseparability. The correspondence between spatial and frequency spectra enables the determination of target coordinates (ρ, z). For further details, please refer to Supplementary Notes 1 and 2.

Drawing inspiration from animals that navigate using electromagnetic wave polarization[39,40], we can also utilize the polarization properties of toroidal fields for positioning purposes. Toroidal fields exhibit space-polarization nonseparability apart from space-time nonseparability[26–29], with their skyrmion polarization textures having been experimentally observed[38]. This intricate spatial topological feature holds the potential for achieving ultrahigh-resolution positioning. Taking TM toroidal pulses as an example, E_ρ exhibits skyrmion-type polarization, as indicated in Fig. 1b4. The azimuthal coordinate θ of the target can be determined based on the polarization characteristics of the electric field vector. Consequently, the time/frequency-polarization information at each 3D spatial point within the primary distribution region of the toroidal field is unique, meaning that it can be uniquely characterized by the time-polarization state or frequency-polarization state. As shown in Fig. 1, by discretizing the 3D space into a grid and placing receivers at each grid point, we can measure the time/frequency-polarization state at each point and store it along with the corresponding spatial coordinates as a positioning information database. Subsequently, by measuring the time/frequency-polarization state at any target spatial point and comparing it with the positioning information database, we can obtain the corresponding spatial coordinates, thus achieving target positioning.

Single-antenna 3D positioning performances

Shen et al. introduced the space and time states as a set of entangled states based on the spatial and temporal properties of toroidal pulses[32]. These states were quantized through measurements of the state density matrix to assess the spatiotemporal inseparability of the toroidal pulses. Inspired by this approach, we define the frequency-polarization amplitude state $|\psi_a\rangle$ and the phase state $|\psi_p\rangle$, leveraging the unique frequency-polarization information at each positioning within the propagation space of the toroidal pulses.

$$|\psi_a\rangle = [|E_{hor}(\lambda, \rho, z, \theta)|, |E_{ver}(\lambda, \rho, z, \theta)|] \quad (4)$$

$$|\psi_p\rangle = \left[\arctan\left(\frac{Im(E_{hor}(\lambda, \rho, z, \theta))}{Re(E_{hor}(\lambda, \rho, z, \theta))}\right), \arctan\left(\frac{Im(E_{ver}(\lambda, \rho, z, \theta))}{Re(E_{ver}(\lambda, \rho, z, \theta))}\right)\right] \quad (5)$$

where, E_{hor} and E_{ver} denote the horizontal and vertical components of the normalized transverse electric field of the toroidal pulses, respectively. We exploit the regularity of the spatial field distribution of the toroidal pulses through measurements of the amplitude of the electric field, and the regularity of its spatial polarization by measuring the phase angles of the electric field components in different directions. Specifically, the frequency-polarization amplitude state encodes information about spatial distance and radial position, while the frequency-polarization phase state contains information about the spatial azimuthal position. Drawing inspiration from the concept of fidelity in quantum mechanics, we introduce a spatial pseudo-spectrum tailored for receiver positioning.

$$F_{tol} = F_a * F_p \quad (6)$$

$$F_a = \frac{\langle\psi_{a,tar}|\psi_{a,pre}\rangle\langle\psi_{a,tar}|\psi_{a,pre}\rangle}{\langle\psi_{a,tar}|\psi_{a,tar}\rangle\langle\psi_{a,pre}|\psi_{a,pre}\rangle} \quad (7)$$

$$F_p = \frac{\langle\psi_{p,tar}|\psi_{p,pre}\rangle\langle\psi_{p,tar}|\psi_{p,pre}\rangle}{\langle\psi_{p,tar}|\psi_{p,tar}\rangle\langle\psi_{p,pre}|\psi_{p,pre}\rangle} \quad (8)$$

where, the subscript "tar" represents the frequency-polarization state measured by the receiver at the target location, while the subscript "pre" denotes the frequency-polarization state obtained from a pre-measured positioning information database at different positions within the area of
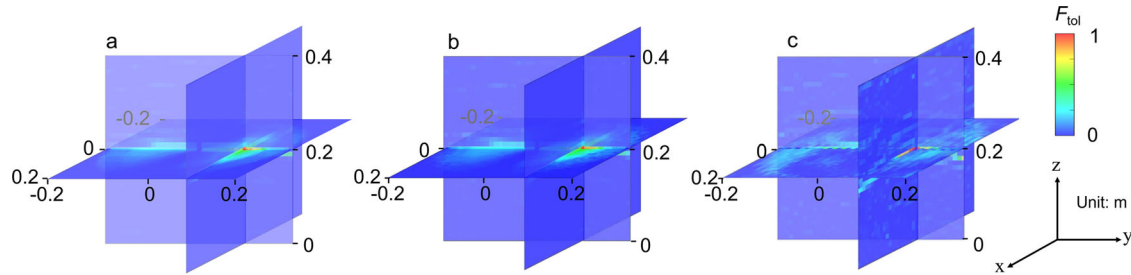
Fig. 2 | Three-dimensional positioning pseudo-spectrum based on toroidal pulses. a Ideal toroidal pulse-based positioning pseudo-spectrum; **b** Positioning pseudo-spectrum computed with toroidal pulses at a signal-to-noise ratio of 20 dB; **c** Experimental positioning pseudo-spectrum constructed from measured data. The target is located at $(x, y, z) = (0, 0.1, 0.2)$ m, with the toroidal pulses propagating in the z-direction and their cross-sectional center located at $(x = 0, y = 0)$.

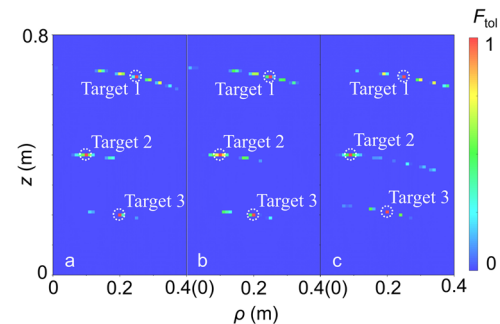interest. In Eqs. (6–8), both F and $|\psi_{pre}\rangle$ are functions of the coordinate positioning (ρ, z, θ), while $|\psi_{tar}\rangle$ is computed based on the signals received by the receiver at the location (ρ_0, z_0, θ_0). Consequently, the computation of F_{tol} using the aforementioned equations yields pseudo-spectrum values for different coordinates (ρ, z, θ), as illustrated in Fig. 2. In Fig. 2, the target is situated at $(x, y, z) = (0, 0.1, 0.2)$ m, with the toroidal pulses propagating in the z-direction, and the frequency range used for computing the pseudo-spectrum is 2–10 GHz.

Figure 2a depicts the theoretical pseudo-spectrum computed using ideal toroidal pulses (given by Eqs. (1–3) with $q_1 = 0.02$ m and $q_2 = 50q_1$). It is evident from the figure that the spatial coordinate corresponding to the maximum pseudo-spectrum value, i.e., 1, aligns with the target location, with high pseudo-spectrum values observed near the target and low values at distant locations. This clearly indicates the target's coordinate. In practical positioning applications, however, test errors due to noise are inevitable. To assess the performance of our method in noisy conditions, we superimposed Gaussian white noise with a signal-to-noise ratio (SNR) of 20 dB on the ideal toroidal pulses field at each position. The recomputed pseudo-spectrum is shown in Fig. 2b, indicating a degree of noise robustness. To validate the positioning method proposed in this study, we conducted experimental tests using a coaxial horn toroidal pulses emitting antenna (Fig. 1b1), as described in ref. 38. Experimental settings are detailed in the Method. The measured 3D pseudo-spectrum is presented in Fig. 2c, clearly identifying the target's coordinate in the experimental results, agreeing well with theoretical predictions.

As observed in Fig. 2, although the maximum value of F_{tol} in the pseudo-spectrum indicates the target's position, the relatively high values of F_{tol} in the vicinity of the target can potentially affect judgment. To improve the purity of the pseudo-spectrum and enhance resolution without compromising positioning accuracy, we can employ techniques to sharpen the pseudo-spectrum. These techniques are described in detail in Supplementary Notes 3 and 4. In addition, it is worth noting that due to the inherent regularity in the spatial-frequency-polarization entanglement of toroidal pulses, we can achieve accurate positioning using spatial pseudo-spectrum computations regardless of the type of receivers.

It is worth noting that only the transversely polarized component of toroidal pulses is utilized in the proposed method because this component exhibits space-time nonseparability and radial polarization characteristics, which are sufficient to ensure the unique correspondence between field and position. In addition, space-time nonseparability is equivalent to space-frequency nonseparability, as discussed in ref. 32, making the theoretical treatment in both time and frequency domains identical. However, defining the frequency-polarization state using the method from ref. 32 is more straightforward. Additionally, from a practical standpoint, recording frequency-domain data enables real-time operation of the positioning system, whereas time-domain data would require recording over a time interval. Therefore, this work adopts the frequency-domain processing method.

In this method, when data is acquired using a point-by-point pre-measurement approach, the database size increases significantly with the expansion of the positioning region. To address this challenge, we propose an aperture field m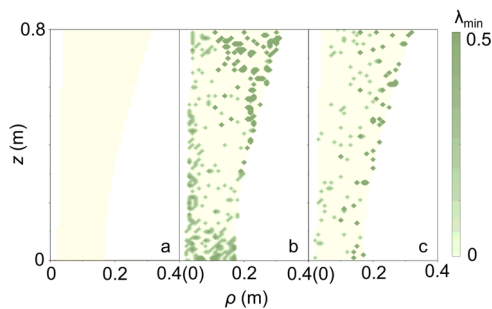ethod, which calculates the field within a space using the field at the aperture of the electromagnetic toroidal pulse emitter, thereby eliminating the need to measure the field at every point in the space. Details of this method are provided in the Supplementary Notes 5–7. Additionally, the proposed method can utilize transmission power similar to that of wireless communication base stations, enabling coverage of a positioning range comparable to their communication range; please refer to the Supplementary Note 8 for the estimation.

Simultaneous positioning of multiple receivers

Beyond the positioning of a single receiver, our method also enables the simultaneous positioning of multiple receivers situated at different locations. By separately computing pseudo-spectra using signals received by different receivers and superimposing the sharpened pseudo-spectra, we can obtain a pseudo-spectrum map for multi-target positioning. Since the pseudo-spectrum values outside the targets' positions are very small, the superimposed pseudo-spectra corresponding to individual receivers do not mutually obscure each other, as demonstrated in Fig. 3. In this figure, the coordinates of targets 1, 2, and 3 are $(r, z) = (0.1, 0.4)$ m, $(0.2, 0.2)$ m, and $(0.25, 0.65)$ m, respectively. Both numerical computations and experimental measurements yield pseudo-spectrum peaks that align with the coordinates of targets.

Evaluation of positioning accuracy

To quantitatively demonstrate the positioning performance of our method, we employed the displacement metric, which quantifies the spatial deviation between the estimated coordinate (derived from the peak of the spatial pseudo-spectrum) and actual target's coordinate. Figure 4 illustrates the displacement when targets are situated at various locations within the primary coverage area of the toroidal pulses. Due to the rotational symmetry of toroidal pulses, examining half of the cylindrical coordinate system along the z-axis suffices to capture their full spatial characteristics. In Fig. 4, the value at each (ρ_0, z_0) coordinate represents the displacement normalized by the shortest wavelength $\lambda_{\min} = 0.03 m$ (corresponding to 10 GHz) used in

Fig. 3 | Multi-target positioning pseudo-spectrum based on toroidal pulses. a Positioning pseudo-spectrum computed using ideal toroidal pulses; **b** Positioning pseudo-spectrum computed using toroidal pulses with a signal-to-noise ratio of 20 dB; **c** Positioning pseudo-spectrum constructed from experimental data.

Fig. 4 | Positioning displacement metrics. a Displacement metrics computed using ideal toroidal pulses; **b** Displacement metrics computed using toroidal pulses with a signal-to-noise ratio of 20 dB; **c** Displacement metrics constructed from experimental data.

the pseudo-spectrum computation, when the actual target's coordinate is (ρ_0, z_0). When utilizing ideal toroidal pulses for positioning, the displacement is zero regardless of the target's coordinate. When the noise with a 20-dB SNR is introduced to toroidal pulses, the displacement remains below $0.5\lambda_{min}$ ($0.3 \lambda_{cen}$ at the central frequency 6 GHz) for 91.82% of the coordinates, indicating robust positioning accuracy even in noisy environments. Experimental results show that 97.15% of the cases are less than $0.5\lambda_{min}$ ($0.3 \lambda_{cen}$) when targets are situated at different locations, consistent with the findings obtained using noisy toroidal pulses. In Supplementary Note 6, we simulated the performance at various noise levels, indicating that higher SNRs lead to better positioning accuracy. In conclusion, owing to space-time nonseparability and skyrmion topology, positioning methods based on toroidal pulses can achieve super-resolution accuracy.

Discussion
By harnessing the inherent space-time nonseparability and skyrmion topology of toroidal pulses, we have realized super-resolution 3D positioning of receivers through the utilization of a solitary toroidal pulse emitting antenna in free space, making the method applicable for various applications including global navigation, mobile communication, automated driving, and others.

It's worth noting that scholars have proposed numerous super-resolution imaging or positioning methods[22,41,42], but their application scenarios differ from freespace microwave positioning. For example, by controlling multipath scattering in reverberation chambers, it is conceivable to achieve super-resolution localization[43–45]. However, this method is unsuitable for freespace microwave positioning, where reverberation scattering is unavailable for exploitation.

The proposed method is also applicable in non-line-of-sight (NLOS) scenarios. In NLOS or multi-scattering linear environments, the effects of scattering cause the frequency-polarization state at any location to become a weighted superposition of multiple frequency-polarization states from free space, thus preserving the uniqueness of each location's frequency-polarization state. Verification cases are provided in Supplementary Note 5.

In addition to the cooperative transmitter-receiver positioning results shown in this paper, the nonseparability and skyrmion topology of toroidal pulses holds promise for pioneering applications in radar detection, internet of things, and penetrative imaging. For scattering scenarios, employing a single coaxial horn antenna to emit toroidal pulses and employing broadband dual-polarization antennas to receive scattered target echoes allows for position determination based on echo polarization and spectral characteristics. By integrating neural network techniques with toroidal pulses, it may even be possible to reconstruct high-precision 3D shapes of targets. Radar or imaging systems based on toroidal pulses offer the potential for higher resolution with simpler system architectures and fewer transceiver units.

As a higher-order form of toroidal pulses, supertoroidal pulses exhibit more pronounced variations in spatial frequency distribution and

polarization distribution[27]. Therefore, utilizing supertoroidal pulses holds promise for constructing higher-resolution positioning, detection, imaging, and other systems. Moreover, supertoroidal pulses may possess non-diffracting propagation characteristics[28], potentially enabling systems based on them to achieve greater effective detection ranges.

Besides the positioning application proposed in the paper, toroidal pulses hold significant promise across a wide array of fields. Their unique properties, such as space-time nonseparability, skyrmion topology, and non-diffracting behavior, open up possibilities in high-capacity tele-communications, where their robust polarization and spectral signatures can enhance data encoding and transmission. Additionally, their potential in developing non-barrel electromagnetic railguns and high-sensitivity sensor systems suggests that toroidal pulses could drive innovation across numerous technological domains, offering transformative solutions beyond traditional methods.

As classical electromagnetic waves, toroidal pulses exhibit identical propagation and topological characteristics across microwave, terahertz, and optical frequency bands. Although this paper primarily discusses the application of toroidal pulses in microwave positioning systems, toroidal pulses have also been generated in the optical and terahertz frequencies[36,37]. Hence, the methodology proposed in this paper also holds potential for applications in optical fields such as nanoscale particle metrology and super-resolution imaging.

Methods
### Numerical positioning method for ideal toroidal pulses
The specific implementation steps of numerical positioning based on ideal toroidal pulses are as follows: (1) Generate an ideal toroidal pulse based on Eqs. (1–3) in Matlab software with $q_1 = 0.02$ m and $q_2 = 50q_1$, setting the propagation axis of the toroidal pulse as the z-axis; (2) Uniformly sample within the region of $x = [-0.4 \ 0.4]$m, $y = [-0.4 \ 0.4]$m, $z = [0 \ 0.8]$m with a 1 cm interval, and record the spectrum of the toroidal pulse at each sampling point; (3) Assume the target is located at Position 0 (ρ_0, z_0, θ_0), use the data recorded at Position 0 (ρ_0, z_0, θ_0) and Position 1 (ρ_1, z_1, θ_1) obtained in step (2) to calculate the pseudo-spectrum value $F_{tol}(\rho_1, z_1, \theta_1)$ at Position 1 (ρ_1, z_1, θ_1) according to Eqs. (4–8); (4) Traverse the coordinates of Position 1 throughout the entire computational domain, repeatedly perform Step (3), and obtain the pseudo-spectrum map of the entire space; (5) Identify the position (ρ_0', z_0', θ_0') with the highest amplitude in the pseudo-spectrum map, which corresponds to the determined target position; (6) Calculate the distance between the determined position (ρ_0', z_0', θ_0') and the actual target position (ρ_0, z_0, θ_0), which represents the positioning displacement value for the target position (ρ_0, z_0, θ_0); (7) Traverse the target Position 0 throughout the entire space, repeatedly perform Steps (3–6), and obtain the positioning displacement value corresponding to each position in the entire space.

Numerical positioning method for noisy toroidal pulses
The specific implementation steps of numerical positioning in the presence of noise are as follows: (1) Follow the same procedure as in the case for ideal toroidal pulse; (2) After step (2) in the ideal toroidal pulse scenario, add two sets of random Gaussian white noise with SNRs of 20 dB to the signals at each position, respectively referred to as pre-measured and target data sets; (3) Assume the target is located at Position 0 (ρ_0, z_0, θ_0), use the data from Position 0 (ρ_0, z_0, θ_0) in the target data set recorded in step (2) and the data from Position 1 (ρ_1, z_1, θ_1) in the pre-measured data set according to Eqs. (4–8) to calculate the pseudo-spectrum value $F_{tol}(\rho_1, z_1, \theta_1)$ at Position 1 (ρ_1, z_1, θ_1); (4) Traverse the coordinates of Position 1 in the pre-measured data set throughout the entire computational domain, repeatedly perform Step (3), and obtain the pseudo-spectrum map of the entire space; (5–6) Follow the same steps as in the ideal toroidal pulse scenario; (7) Traverse the target Position 0 throughout the entire space in the target data set, repeatedly perform Steps (3–6), and obtain the positioning displacement value corresponding to each position in the entire space.

Fig. 5 | Experimental setup. The experimental setup utilized coaxial horn antennas as the transmitting antennas for toroidal fields, while double-ridged waveguide horn antennas served as the dual-polarized receiving antennas, simulating the user positionings to be localized, as shown in (**a**). **b** Schematic of the coaxial horn antenna transmitting microwave toroidal pulses. The green and black represent dielectric support structures and metallic coaxial horn, respectively.
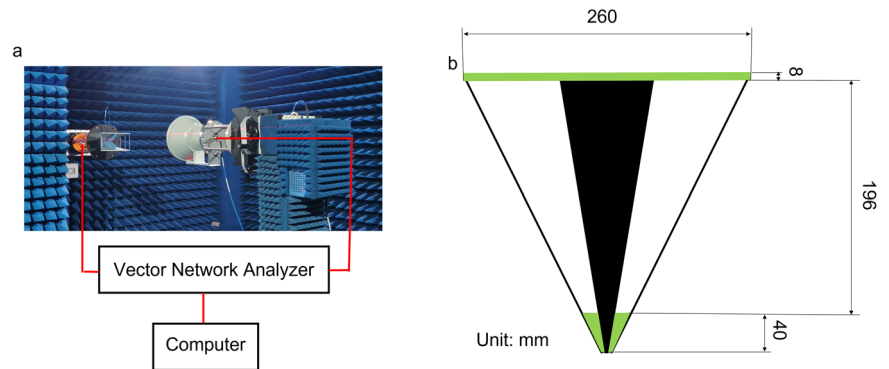
Experimental positioning method

The TM toroidal pulses transmitter employed in the experimental validation of the proposed positioning technology is a coaxial horn antenna proposed in ref. 38. The experimental setup utilized coaxial horn antennas operating within the frequency range of 1.3–10 GHz as the transmitting antennas for toroidal fields, while double-ridged waveguide horn antennas (operating within 1–18 GHz) served as the dual-polarized receiving antennas, simulating the user to be localized. The geometric center of the coaxial horn antenna aperture was designated as the origin of the cylindrical coordinate system. The experimental frequency range was set to 2–10 GHz, with the spatial z-axis originated at a distance of 0.2 m from the coaxial horn antenna. Under identical experimental conditions, the spatial E_ρ distribution was measured twice. The amplitude and phase deviations between the two experimental datasets were found to be within 1%–2%. The experimental system was situated in a planar field measurement chamber, as depicted in Fig. 5a, where the transmitting and receiving antennas were connected to a vector network analyzer and controlled by a computer. The double-ridged waveguide horn antenna could be moved in 3D space using a rail system, simulating various user coordinates. Figure 5b illustrates the cross-sectional structure of the coaxial horn antenna, where a 180° rotation along the symmetry axis reveals the complete antenna geometry. The black color represents the metal conductor, while the green color indicates a material with a dielectric constant of 1.3, serving to support the inner and outer conductors of the coaxial horn antenna. The antenna is fed through a coaxial cable connected at its base.

The procedure for obtaining experimental positioning results is as follows: (1) A 2–10 GHz signal is fed into the coaxial horn toroidal field transmitter, with the central axis of the coaxial horn set as the z-axis and the aperture of the horn set at $z = 0$; (2) Spectra are measured at each spatial position within the region of $x = [-0.4\ 0.4]$m, $y = [-0.4\ 0.4]$ m, $z = [0\ 0.8]$ m at 1 cm intervals, and recorded as the pre-measured data set; (3) The target under test is placed at Position 0 (ρ_0, z_0, θ_0), and the spectrum is re-measured, representing the received signal spectrum when the target is located at Position 0. Using this re-measured spetrum and the data from Position 1 (ρ_1, z_1, θ_1) in the pre-measured data set, the pseudo-spectrum value $F_{tol}(\rho_1, z_1, \theta_1)$ at Position 1 (ρ_1, z_1, θ_1) is calculated according to Eqs. (4–8); (4–6) Follow the same steps as in the case of positioning with noisy toroidal pulse; (7) The target under test is placed at different positions through the entire space, repeating Steps (3–6) continuously to obtain the positioning displacement value corresponding to each position.

Data availability

The data that support the findings of this study are available from the corresponding author upon reasonable request.

Code availability

The code that supports the findings of this study is available from the corresponding author upon reasonable request.

References

1. Prescott, W. H., Davis, J. L. & Svarc, J. L. Global positioning system measurements for crustal deformation: precision and accuracy. *Science* **244**, 1337–1340 (1989).
2. Giles, J. EU plans global positioning system. *Nature* **410**, 853–853 (2001).
3. Elsheikh, M., Iqbal, U., Noureldin, A. & Korenberg, M. The implementation of precise point positioning (PPP): a comprehensive review. *Sensors* **23**, 8874 (2023).
4. Kentosh, J. & Mohageg, M. Global positioning system test of the local position invariance of Planck's constant. *Phys. Rev. Lett.* **108**, 110801 (2012).
5. Rizos, C. & Yang, L. Background and recent advances in the Locata terrestrial positioning and timing technology. *Sensors* **19**, 1821 (2019).
6. Humphreys, T. E., Murrian, M. J. & Narula, L. Deep-urban unaided precise global navigation satellite system vehicle positioning. *IEEE Intell. Transp. Syst. Mag.* **12**, 109–122 (2020).
7. Giovannetti, V., Lloyd, S. & Maccone, L. Quantum-enhanced positioning and clock synchronization. *Nature* **412**, 417–419 (2001).
8. del Peral-Rosado, J. A., Raulefs, R., López-Salcedo, J. A. & Seco-Granados, G. Survey of cellular mobile radio localization methods: from 1G to 5G. *IEEE Commun. Surveys Tuts.* **20**, 1124–1148 (2017).
9. Janssen, T., Koppert, A., Berkvens, R. & Weyn, M. A survey on IoT positioning leveraging LPWAN, GNSS and LEO-PNT. *IEEE Internet Things J.* **10**, 11135–11159 (2023).
10. Chen, H. et al. Phone signals can help you find your way in cities even without GPS. *Nature* **611**, 454–455 (2022).
11. Koelemeij, J. C. J. et al. A hybrid optical–wireless network for decimetre-level terrestrial positioning. *Nature* **611**, 473–478 (2022).
12. Nye, J. F. & Berry, M. V. Dislocations in wave trains. In: A Half-Century of Physical Asymptotics and Other Di-versions: Selected Works by Michael Berry, 6–31 (World Scientific, 1974).
13. Willner, A. E., Pang, K., Song, H., Zou, K. & Zhou, H. Orbital angular momentum of light for communications. *Appl. Phy. Rev.* **8**, 041312 (2021).
14. Berry, M. Making waves in physics. *Nature* **403**, 21–21 (2000).
15. Bliokh, K. Y. et al. Roadmap on structured waves. *J. Opt.* **25**, 103001 (2023).
16. Wan, Z., Wang, H., Liu, Q., Fu, X. & Shen, Y. Ultra-degree-of-freedom structured light for ultracapacity information carriers. *ACS Photonics* **10**, 2149–2164 (2023).
17. Wan, Z. et al. Divergence-degenerate spatial multiplexing towards future ultrahigh capacity, low error-rate optical communications. *Light Sci. Appl.* **11**, 144 (2022).
18. Pryamikov, A. Rising complexity of the OAM beam structure as a way to a higher data capacity. *Light Sci. Appl.* **11**, 221 (2022).

19. Berg-Johansen, S. et al. Classically entangled optical beams for high-speed kinematic sensing. *Optica* **2**, 864–868 (2015).
20. Yuan, G. H. & Zheludev, N. I. Detecting nanometric displacements with optical ruler metrology. *Science* **364**, 771–775 (2019).
21. Vettenburg, T. et al. Light-sheet microscopy using an Airy beam. *Nat. Methods* **11**, 541–544 (2014).
22. Zheludev, N. I. & Yuan, G. Optical superoscillation technologies beyond the diffraction limit. *Nat. Rev. Phys.* **4**, 16–32 (2022).
23. Jia, S., Vaughan, J. C. & Zhuang, X. Isotropic three-dimensional super-resolution imaging with a self-bending point spread function. *Nat. Photonics* **8**, 302–306 (2014).
24. Miao, Pei et al. Orbital angular momentum microlaser. *Science* **353**, 464–467 (2016).
25. Hellwarth, R. W. & Nouchi, P. Focused one-cycle electromagnetic pulses. *Phy. Rev. E* **54**, 889 (1996).
26. Shen, Y. et al. Roadmap on spatiotemporal light fields. *J. Opt.* **25**, 093001 (2023).
27. Shen, Y., Hou, Y., Papasimakis, N. & Zheludev, N. I. Supertoroidal light pulses as electromagnetic skyrmions propagating in free space. *Nat. Commun.* **12**, 5891 (2021).
28. Shen, Y., Papasimakis, N., & Zheludev, N. I. Nondiffracting supertoroidal pulses: optical "Kármán vortex streets". *Nat. Commun.* **15**, 4863 (2024).
29. Kaelberer, T., Fedotov, V. A., Papasimakis, N., Tsai, D. P. & Zheludev, N. I. Toroidal dipolar response in a metamaterial. *Science* **330**, 1510–1512 (2010).
30. He, C., Shen, Y. & Forbes, A. Towards higher-dimensional structured light. *Light Sci. Appl.* **11**, 205 (2022).
31. Shen, Y. & Rosales-Guzmán, C. Nonseparable states of light: from quantum to classical. *Laser Photonics Rev.* **16**, 2100533 (2022).
32. Shen, Y., Zdagkas, A., Papasimakis, N. & Zheludev, N. I. Measures of space-time nonseparability of electromagnetic pulses. *Phy. Rev. Res.* **3**, 013236 (2021).
33. Shen, Y. et al. Optical skyrmions and other topological quasiparticles of light. *Nat. Photonics* **18**, 15–25 (2024).
34. Papasimakis, N. et al. Electromagnetic toroidal excitations in matter and free space. *Nat. Mater.* **15**, 263–271 (2016).
35. Raybould, T., Fedotov, V. A., Papasimakis, N., Youngs, I. & Zheludev, N. I. Exciting dynamic anapoles with electromagnetic doughnut pulses. *Appl. Phy. Lett.* **111**, 081104 (2017).
36. Zdagkas, A. et al. Observation of toroidal pulses of light. *Nat. Photonics* **16**, 523–528 (2022).
37. Jana, K. et al. Quantum control of flying doughnut terahertz pulses. *Sci. Adv.* **10**, eadl1803 (2024).
38. Wang, R. et al. Observation of resilient propagation and free-space skyrmions in toroidal electromagnetic pulses. *Appl. Phys. Rev.* **11**, 031411 (2024).
39. Powell, S. B., Garnett, R., Marshall, J., Rizk, C. & Gruev, V. Bioinspired polarization vision enables underwater geolocalization. *Sci. Adv.* **4**, eaao6841 (2018).
40. Graydon, O. Global position by polarization. *Nat. Photonics* **12**, 318–318 (2018).
41. Power, R. M., Tschanz, A., Zimmermann, T. & Ries, J. Build and operation of a custom 3D, multicolor, single-molecule localization microscope. *Nat. Protoc.* **686**, 1–59 (2024).
42. Astratov, V. N. et al. Roadmap on label-free super-resolution imaging. *Laser Photonics Rev.* **17**, 2200029 (2023).
43. Cohen, S. D., Cavalcante, H. L. D. S. & Gauthier, D. J. Subwavelength position sensing using nonlinear feedback and wave chaos. *Phys. Rev. Lett.* **107**, 254103 (2011).
44. Del Hougne, P., Imani, M. F., Fink, M., Smith, D. R. & Lerosey, G. Precise localization of multiple noncooperative objects in a disordered cavity by wave front shaping. *Phys. Rev. Lett.* **121**, 063901 (2018).
45. Gigan, S. & Del Hougne, P. Deeply subwavelength localization with reverberation-coded aperture. *Phys. Rev. Lett.* **127**, 043903 (2021).

Acknowledgements

Author contributions
R.W. conceived the ideas and supervised the project, R.W., P.Y.B., X. F., and J. W. performed the theoretical modeling and numerical simulations, R.W. developed the experimental methods, P.Y.B. and R.W. conducted the experimental measurements, R.W., P.Y.B., B.Z.W., and Y.S. conducted data analysis. All authors wrote the manuscript and participated in the discussions.

Competing interests
The authors declare no competing interests.

Additional information
Supplementary information The online version contains supplementary material available at https://doi.org/10.1038/s42005-024-01850-z.

Correspondence and requests for materials should be addressed to Ren Wang or Yijie Shen.

Peer review information *Communications Physics* thanks the anonymous reviewers for their contribution to the peer review of this work. A peer review file is available.

Reprints and permissions information is available at http://www.nature.com/reprints

Publisher's note Springer Nature remains neutral with regard to jurisdictional claims in published maps and institutional affiliations.